Transmitter Precoding Aided Spatial Modulation Achieving Both Transmit and Receive Diversity

Chaowen Liu, Lie-Liang Yang, *Fellow, IEEE*, and Wenjie Wang, *Member, IEEE*

***Abstract*—We propose and investigate a precoding-aided spatial modulation (PSM) scheme, which can simultaneously achieve transmit and receive diversity and, hence, is referred to as the TRD-PSM scheme. In TRD-PSM systems, information is transmitted jointly using an amplitude-phase modulation (APM) and a receive antenna based space-shift keying (SSK) modulation. We consider two types of linear precoders, namely transmitter zero-forcing (TZF) and transmitter minimum mean-square error (TMMSE), so as to facilitate low-complexity signal detection. In order to satisfy the different requirement for complexity and reliability, we introduce/propose a range of detection algorithms, which include joint maximum likelihood detector (JMLD), simplified JMLD, successive MLD (SMLD), simplified SMLD, and *ratio threshold test* assisted MLD (RTT-MLD). We address the principles, characteristics, complexity and performance of these detection algorithms. Furthermore, we analyze the average bit error probability (ABEP) of the TZF- and TMMSE-assisted TRD-PSM systems employing respectively the JMLD and simplified JMLD and at both small- and large-scale. Finally, numerical and simulation results are provided to demonstrate and compare the achievable performance of TRD-PSM systems employing various precoding and detection algorithms, as well as to validate the formulas derived.**

***Index Terms*—Multiple-input multiple-output (MIMO), spatial modulation, precoding, precoding assisted spatial modulation, diversity, average bit error probability, asymptotic analysis.**

I. Introduction

In order to attain low-complexity and energy-efficient multiple-input multiple-output (MIMO) systems, various space-relied modulation schemes have been proposed and investigated in recent years, as witnessed by [1–4] and the references therein. With one or a fraction of transmit/receive antennas being activated to modulate information in the spatial domain, spatial modulation (SM) schemes have the capability to relax the requirement for inter-antenna-synchronization (IAS), to mitigate inter-channel-interference (ICI), to reduce the number of radio frequency up-conversion chains, or to achieve lower complexity detection, in contrast to the conventional MIMO schemes. Owing to these advantages, SM has been studied from different perspectives, again, as shown in [1–4] and the references therein.

Copyright (c) 2015 IEEE. Personal use of this material is permitted. However, permission to use this material for any other purposes must be obtained from the IEEE by sending a request to pubs-permissions@ieee.org.

C. Liu and W. Wang are with the Ministry of Education Key Laboratory for Intelligent Networks and Network Security, Xi'an Jiaotong University, Xi'an, 710049, Shaanxi, China. (E-mail: liucwhb@gmail.com, wjwang@mail.xjtu.edu.cn)

L.-L. Yang is with the Southampton Wireless Group, School of Electronics and Computer Science, University of Southampton, Southampton SO17 1BJ, UK. (E-mail: lly@ecs.soton.ac.uk, http://users.ecs.soton.ac.uk/lly/)

In literature, there are various SM schemes. As some examples, in [5–8] the authors have proposed to use the indices of transmit antennas for information modulation, forming the space-shift keying (SSK) scheme. In the general form of spatial modulation (SM) [5–7, 9–13], information is jointly transmitted by an amplitude-phase modulation (APM), such as, phase-shift keying (PSK), quadrature-amplitude modulation (QAM), etc., and a SSK modulation. In [14], a space-time shift keying (STSK) modulation has been proposed, which conveys information by jointly making use of the degrees of freedom provided by the space and time domains, as well as the conventional APM constellations. Furthermore, in [10], SM has been integrated with orthogonal frequency division multiplexing (OFDM) for information delivery.

Corresponding to the various SM schemes, different types of detectors have been proposed, in order to achieve a good trade-off between reliability and complexity, as seen, e.g., in the above-mentioned references and [11, 15, 16]. Furthermore, the performance of SM systems with various detection approaches has been studied. Specifically, in [17], the authors have analyzed the error performance of the SSK modulated systems, when assuming communications over correlated and non-identical Nakagami-m fading channels. The asymptotic error performance of SM systems has been analyzed in [18], when assuming a Nakagami-m fading channel model. In [19], the authors have analyzed the error performance of the SM systems communicating over generic fading channels, which provides a comprehensive framework for analyzing the average bit error probability (ABEP) of SM systems.

As a counterpart to the SM, a precoding aided spatial modulation (PSM) scheme has been introduced in [20], which uses the indices of receive antennas for delivery of extra information. Based on the principles of PSM, different PSM schemes have been proposed and investigated, and some of them are referred to as the receive spatial modulation (RSM) [21–25]. In more detail, by introducing the RSM to the multi-user MIMO, the authors of [21] have proposed and investigated a multistream RSM scheme. With the aid of the high signal-to-noise ratio (SNR) approximation, the asymptotic error performance of the multistream RSM systems has been analyzed in [22], where both small- and large-scale fading are taken into account. The authors of [23] have analyzed the symbol error rate, diversity order, and the coding gain of the RSM-assisted MIMO systems, when assuming shadowing broadcast channels. In order to enhance the spectral efficiency of the MIMO spatial multiplexing (SMX) system, a dual-layered transmission scheme has been proposed in [24], where RSM is applied to a joint spatial and power-level

domain. In [25], a hybrid SM-assisted relay scheme has been composed, where a RSM is implemented for the source-to-relay transmission, and a SM is used for supporting the relay-to-destination transmission. The generalization of PSM, i.e., GPSM, has been addressed in [26]. Instead of activating one receive antenna in the PSM, the GPSM activates multiple receive antennas during each symbol duration for attaining a higher data rate. Subsequently, the capacity and achievable rate of the GPSM systems have been analyzed, when the joint optimal detection and the decoupled sub-optimal detection are respectively employed [27]. By transplanting the philosophy of GPSM into internet-of-things architectures, in [28], the author has proposed a network topology modulation scheme, which enables the simultaneous energy and data transmission for the internet of magneto-inductive things. In the PSM/GPSM schemes, typically, liner precoding has been employed for activating the intended receive antenna(s) [20–22, 24–27, 29]. By contrast, in [30], a non-linear precoding aided GPSM scheme has been proposed and studied, which is capable of further enhancing the error performance of the GPSM.

While the SM schemes can readily attain receive diversity in the case that multiple receive antennas are employed, achieving transmit diversity in SM schemes is not straightforward. In [31–35], by assuming CSI at transmitter (CSIT), transmitter preprocessing aided SM schemes have been proposed, in order to simultaneously achieve both transmit and receive diversity. By contrast, according to the principles of PSM/GPSM (or RSM), transmit diversity is always available, provided that the number of transmit antennas is higher than the number of receive antennas. However, to the best of the authors' knowledge, there are rarely prior works in PSM, which have considered to employ additional receive antennas for achieving receive diversity. In [29], the author has proposed a PSM scheme for operation in the scenario, where the number of receive antennas is more than the number of transmit antennas. In order to implement the original PSM [20] in this case, a subset of receive antennas[1] are selected based on the full channel state information (CSI) known to the transmitter. Explicitly, this PSM transmission scheme is capable of attaining receive selection diversity. However, implementing the propose PSM scheme with optimal detection requires that both the transmitter and receiver have to employ full CSI, which is highly challenging in practice. Moreover, in order to select an optimum subset of receive antennas, a search algorithm involving matrix inversion has to be conducted over all possible antenna combinations for subsets. This results in extreme complexity and possibly high latency, especially, when the number of receive antennas is high.

Against the background, in this treatise, we propose a PSM scheme, which may achieve both transmit(T)- and receive(R)-diversity (D), and hence is referred to as the TRD-PSM system. In the TRD-PSM system, a subset of receive antennas are fixed for encoding the spatial information, while the remaining receive antennas are utilized for providing receive diversity. In contrast to the PSM scheme proposed in [29], which demands full CSI for the transmitter to dynamically choose a subset of receive antennas, in our TRD-PSM system, the transmitter only expects the part of CSI required for carrying out precoding, as seen in our forthcoming discourses. In the TRD-PSM system, the transmitter is not required to dynamically identify a subset of receive antennas for encoding spatial information. Hence, the complexity of the TRD-PSM transmitter can be significantly lower than that of the PSM transmitter in [29]. Furthermore, the TRD-PSM scheme imposes no constraint on the relationship between the number of transmit antennas and the number of receive antennas, provided that the system has multiple transmit antennas and multiple receive antennas, i.e., is a MIMO system. In this case, for any given number (> 1) of transmit antennas, an appropriate subset of receive antennas is always available for implementing a PSM with, e.g., linear precoding. After the selection, the remaining receive antennas can be exploited to achieve receive diversity, which enhances error performance, or can be used to trade for a higher rate APM. Owing to its merits, the TRD-PSM scheme may be flexibly implemented with various MIMO scenarios, e.g., uplink or downlink, provided that the required CSI is available for the transmission and detection.

In addition to the above-mentioned, the other novelty and main contributions of the paper can be summarized as follows.

- A TRD-PSM system is proposed, in which a subset of receive antennas are used for implementing the PSM, while the other receive antennas are exploited for achieving receive diversity. In addition to the receive diversity, the TRD-PSM system can also attain transmit diversity, if the number of receive antennas in the subset is less than the number of transmit antennas. In our TRD-PSM system, transmit diversity is achieved with the aid of precoding in the principles of, e.g., zero-forcing (ZF) or minimum mean-square error (MMSE), which are referred to as TZF or TMMSE for convenience. By contrast, receive diversity is obtained through the employment of high-efficiency detection algorithms, as noted below.
- In order to meet different levels of requirement for reliability and complexity, a range of detectors are introduced. In detail, we first introduce the joint maximum likelihood detector (JMLD), which achieves the best error performance, but also demands the highest complexity for implementation. Second, by assuming TZF or TMMSE, we reduce the JMLD to a simplified JMLD, which has slightly lower complexity than the JMLD. Third, in order to further decrease the detection complexity, we *propose* a successive MLD (SMLD) and also reduce it to the simplified SMLD. This simplified SMLD is in fact a detector widely employed in the SM/PSM systems proposed in references, e.g., in [10, 11, 15, 16, 26]. However, our studies in this paper show that this simplified SMLD is inefficient and yields significant performance degradation, when it is operated in the PSM systems, where only a subset of receive antennas are used for SSK modulation. Finally, for the sake of achieving a best possible trade-off between error performance and complexity, we *propose* a ratio threshold test assisted MLD (RTT-MLD). In the

[1]The number of receive antennas in the subset should not exceed the number of transmit antennas in order to implement linear precoding.

RTT-MLD, a search space having significantly smaller size than that of the JMLD is first identified based on the principles of RTT [36–39]. Then, the information conveyed by the SSK and APM is jointly detected using a MLD operated in the identified search space. Our studies and performance results show that both the SMLD and RTT-MLD are high-efficiency detection schemes in terms of the trade-off between complexity and reliability.

- In order to gain the insight into the TRD-PSM system's characteristics and its performance limit, we analyze the ABEP of TRD-PSM systems employing respectively the JMLD and simplified JMLD. In our analysis, both small- and large-scale TRD-PSM systems are considered. For the small-scale TRD-PSM systems, the approximate ABEP expressions are derived by analyzing the union-bound with the aid of the Gamma approximation (Gamma-Ap). By contrast, for the large-scale TRD-PSM systems, we derive the asymptotic ABEP formulas by imposing the large-scale approximations. All the analytical expressions are validated by simulation results. As our studies and performance results show, the approximate and asymptotic ABEP expressions derived in this paper are general, which are suitable for the PSM systems without using diversity antennas at receiver. This can be achieved simply by letting the number of diversity antennas equal to zero.

The remainder of the paper is structured as follows. In Section II, we describe the TRD-PSM systems employing TZF and TMMSE. This is followed by proposing a range of detectors in Section III. Section IV analyzes the ABEP of the TRD-PSM systems employing respectively the JMLD and simplified JMLD. Our performance results and related discussions are provided in Section V. Finally, we summarize the main observations in Section VI.

Notations: Boldface upper-case and lower-case letters represent matrices and vectors, respectively. $\mathbb{E}[\cdot]$ and $\mathrm{Tr}(\cdot)$ denote respectively statistical expectation and square-matrix's trace. $\boldsymbol{A}^H$, $\boldsymbol{A}^T$, $\boldsymbol{A}^*$ and $\boldsymbol{A}^{-1}$ stand for Hermitian transpose, transpose, conjugate and inverse of matrix $\boldsymbol{A}$. $\boldsymbol{I}_M$ is a $(M \times M)$ identity matrix. $\Re\{x\}$ and $|x|$ take respectively the real part and modulus of x. $\|\boldsymbol{a}\|$ denotes the Euclidean norm of vector $\boldsymbol{a}$, while $P_r\{\cdot\}$ denotes the statistical probability calculator.

II. System Model

The TRD-PSM system considered is a point-to-point PSM-modulated MIMO system, whose transmitter and receiver are equipped with $N > 1$ and $M > 1$ antennas, respectively. Let the $(N \times M)$ channel matrix of this PSM system be expressed as $\boldsymbol{H} = [\boldsymbol{h}_0, \boldsymbol{h}_1, \cdots, \boldsymbol{h}_{M-1}]$, where $\boldsymbol{h}_m$, $m \in \{0, 1, \ldots, M-1\}$, is an N-length column vector containing the channel gains from the N transmit antennas to the mth receive antenna. We assume that the transmitter is capable of acquiring the CSI required for carrying out precoding, while the receiver has the required CSI for detection. In literature, almost all the existing PSM-related research works assume that all receive antennas are exploited to bear spatial information. In this paper, we relax this constraint and assume that a part of receive antennas are utilized to encode spatial information, while the remaining receive antennas are used to attain receive diversity.

Let $M_1 = 2^{k_1}$ out of the M receive antennas be used for information delivery, while the other $M_d = (M - M_1)$ receive antennas be used for achieving receive diversity. In order to carry out linear transmitter precoding, such as the TZF, TMMSE, etc. [20], and to achieve transmit diversity, we assume that $M_1 \leq N$. Correspondingly, the $(N \times M_1)$ channel matrix is expressed as $\boldsymbol{H}_1 = [\boldsymbol{h}_0, \boldsymbol{h}_1, \cdots, \boldsymbol{h}_{M_1-1}]$, which are constituted by the M_1 columns of $\boldsymbol{H}$ chosen according to a given optimization strategy. Therefore, $\boldsymbol{H}_1$ is not necessarily constituted by the first M_1 columns of $\boldsymbol{H}$. However, for convenience of description, we simply assume that the first M_1 receive antennas are used for information configuration based on the M_1-ary SSK (M_1-SSK), while the rest M_d receive antennas are used to achieve receive diversity. Let the transmitter precoding matrix designed based on $\boldsymbol{H}_1$ be expressed as $\boldsymbol{P} = [\boldsymbol{p}_0, \boldsymbol{p}_1, \cdots, \boldsymbol{p}_{M_1-1}]$, which is an $(N \times M_1)$ matrix and is normalized to satisfy $\mathrm{Tr}(\boldsymbol{P}\boldsymbol{P}^H) = M_1$. Let $m_1 \in \mathcal{M}_1 = \{0, 1, \cdots, M_1 - 1\}$ be an integer determined by k_1 binary bits delivered by the M_1-SSK, and $x \in \mathcal{X} = \{X_0, X_1, \cdots, X_{M_2-1}\}$ be an M_2-ary APM (M_2-APM) symbol, such as PSK, QAM symbol, determined by another $k_2 = \log_2 M_2$ binary bits. Furthermore, we assume that the signals in $\mathcal{X}$ satisfy $\mathbb{E}\{|X_i|^2\} = 1$. Then, following the principles of PSM as shown in [20], we can write the discrete signals transmitted from the N transmit antennas as

$$\boldsymbol{s} = \boldsymbol{p}_{m_1} x \tag{1}$$

which conveys $(k_1 + k_2)$ bits per symbol.

When $\boldsymbol{s}$ is transmitted over the MIMO channels defined by $\boldsymbol{H}$, the received observation at the mth receive antenna is given by

$$\begin{aligned} y_m = \boldsymbol{h}_m^T \boldsymbol{s} + n_m = \boldsymbol{h}_m^T \boldsymbol{p}_{m_1} x + n_m, \\ m = 0, 1, \ldots, M-1 \end{aligned} \tag{2}$$

and the observations from the M receive antennas can be expressed as

$$\boldsymbol{y} = \boldsymbol{H}^T \boldsymbol{p}_{m_1} x + \boldsymbol{n} \tag{3}$$

where, by definition,

$$\begin{aligned} \boldsymbol{y} &= [y_0, y_1, \cdots, y_{M-1}]^T \\ \boldsymbol{n} &= [n_0, n_1, \cdots, n_{M-1}]^T \end{aligned} \tag{4}$$

In (4), $\boldsymbol{n}$ obeys the complex Gaussian distribution with zero mean and an $(M \times M)$ covariance matrix of $\sigma^2 \boldsymbol{I}_M$, where $\sigma^2 = 1/\gamma_s = [(k_1 + k_2)\gamma_b]^{-1}$ with γ_s and γ_b denoting the average signal-to-noise ratio (SNR) per symbol and per bit, respectively.

Furthermore, let us express $\boldsymbol{H} = [\boldsymbol{H}_1, \boldsymbol{H}_d]$, where $\boldsymbol{H}_d$ is an $(N \times M_d)$ channel matrix from the N transmit antennas to the M_d diversity antennas. Correspondingly, when we divide $\boldsymbol{y}$ and $\boldsymbol{n}$ into $\boldsymbol{y} = [\boldsymbol{y}_1^T, \boldsymbol{y}_d^T]^T$ and $\boldsymbol{n} = [\boldsymbol{n}_1^T, \boldsymbol{n}_d^T]^T$, we have

$$\boldsymbol{y}_1 = \boldsymbol{H}_1^T \boldsymbol{p}_{m_1} x + \boldsymbol{n}_1 \tag{5}$$

$$\boldsymbol{y}_d = \boldsymbol{H}_d^T \boldsymbol{p}_{m_1} x + \boldsymbol{n}_d \tag{6}$$

where $\boldsymbol{y}_1$ contains the observations from the M_1 receive antennas used to identify the M_1-SSK symbol, while $\boldsymbol{y}_d$ contains the other observations from the M_d diversity antennas, which serves the purpose of performance enhancement.

As shown in [20], when the TZF-assisted TRD-PSM (TZF/TRD-PSM) is applied, the precoding matrix is given by

$$\boldsymbol{P} = \beta \boldsymbol{H}_1^* \left(\boldsymbol{H}_1^T \boldsymbol{H}_1^*\right)^{-1} \tag{7}$$

where $\beta = \sqrt{M_1/\mathrm{Tr}((\boldsymbol{H}_1^T\boldsymbol{H}_1^*)^{-1})}$. By contrast, when the TMMSE-assisted TRD-PSM (TMMSE/TRD-PSM) is employed, we have

$$\boldsymbol{P} = \beta' \left(\boldsymbol{H}_1^* \boldsymbol{H}_1^T + M_1\sigma^2 \boldsymbol{I}_N\right)^{-1} \boldsymbol{H}_1^* \tag{8}$$

$$= \beta' \boldsymbol{H}_1^* \left(\boldsymbol{H}_1^T \boldsymbol{H}_1^* + M_1\sigma^2 \boldsymbol{I}_{M_1}\right)^{-1} \tag{9}$$

where, corresponding to (8) and (9), we have $\beta' = \sqrt{M_1/\mathrm{Tr}((\boldsymbol{H}_1^*\boldsymbol{H}_1^T + M_1\sigma^2\boldsymbol{I}_N)^{-2}\boldsymbol{H}_1^*\boldsymbol{H}_1^T)}$ and $\beta' = \sqrt{M_1/\mathrm{Tr}((\boldsymbol{H}_1^T\boldsymbol{H}_1^* + M_1\sigma^2\boldsymbol{I}_{M_1})^{-2}\boldsymbol{H}_1^T\boldsymbol{H}_1^*)}$, respectively. From (7), (8) and (9) we can know that the transmitter only requires the CSI of $\boldsymbol{H}_1$ for implementation of the PSM, instead of the whole CSI of $\boldsymbol{H}$ as in [20]. Therefore, given the constraints on the implementation complexity and on the resource available for a transmitter to acquire CSI, we have the flexibility to choose the number of receive antennas for PSM in the design of a TRD-PSM system. This flexibility may provide us a best trade-off among the implementation complexity, overhead and the achievable performance.

When the TZF/TRD-PSM is employed, and upon substituting (7) into (5), we can obtain

$$\boldsymbol{y}_1 = \beta \boldsymbol{e}_{m_1} x + \boldsymbol{n}_1 \tag{10}$$

where $\boldsymbol{e}_{m_1}$ is the m_1th column of $\boldsymbol{I}_{M_1}$. In more detail, (10) gives

$$\begin{aligned} y_{m_1} &= \beta x + n_{m_1}, \\ y_m &= n_m, \ m = 0, 1, \ldots, M_1 - 1 \text{ and } m \neq m_1 \end{aligned} \tag{11}$$

In the context of the TMMSE/TRD-PSM, let in (8) $\boldsymbol{P} = \beta'\tilde{\boldsymbol{P}}$, where $\tilde{\boldsymbol{P}} = [\tilde{\boldsymbol{p}}_0, \tilde{\boldsymbol{p}}_1, \cdots, \tilde{\boldsymbol{p}}_{M_1-1}]$. Then, upon submitting $\boldsymbol{P} = \beta'\tilde{\boldsymbol{P}}$ into (5), we obtain the M_1-length decision variable vector

$$\boldsymbol{y}_1 = \beta' \boldsymbol{H}_1^T \tilde{\boldsymbol{p}}_{m_1} x + \boldsymbol{n}_1 \tag{12}$$

which can be expressed individually as

$$\begin{aligned} y_{m_1} &= \beta' \boldsymbol{h}_{m_1}^T \tilde{\boldsymbol{p}}_{m_1} x + n_{m_1}, \\ y_m &= \beta' \boldsymbol{h}_m^T \tilde{\boldsymbol{p}}_{m_1} x + n_m, \\ & m = 0, \ldots, M_1 - 1, \text{ and } m \neq m_1 \end{aligned} \tag{13}$$

Furthermore, from (8), we can derive for $m = 0, 1, \ldots, M_1 - 1$ that

$$\tilde{\boldsymbol{p}}_m = \left(\boldsymbol{H}_1^* \boldsymbol{H}_1^T + M_1\sigma^2 \boldsymbol{I}_N\right)^{-1} \boldsymbol{h}_m^* \tag{14}$$

Substituting it into (13), the M_1 decision variables generated by the TMMSE/TRD-PSM can be written as

$$\begin{aligned} y_{m_1} &= \beta' \boldsymbol{h}_{m_1}^T \left(\boldsymbol{H}_1^* \boldsymbol{H}_1^T + M_1\sigma^2 \boldsymbol{I}_N\right)^{-1} \boldsymbol{h}_{m_1}^* x + n_{m_1}, \\ y_m &= \beta' \boldsymbol{h}_m^T \left(\boldsymbol{H}_1^* \boldsymbol{H}_1^T + M_1\sigma^2 \boldsymbol{I}_N\right)^{-1} \boldsymbol{h}_{m_1}^* x + n_m, \\ & m = 0, 1, \ldots, M_1 - 1, \text{ and } m \neq m_1 \end{aligned} \tag{15}$$

Equation (15) shows that the decision variable matching to the transmitted symbol contains both the desired signal and the Gaussian noise, while the other decision variables contain the Gaussian noise and the interference resulted from the TMMSE precoding. According to [40], after the processing in MMSE principles, the resultant interference can be closely approximated as Gaussian noise. Therefore, let $\beta = \beta' \boldsymbol{h}_{m_1}^T (\boldsymbol{H}_1^* \boldsymbol{H}_1^T + M_1\sigma^2 \boldsymbol{I}_N)^{-1} \boldsymbol{h}_{m_1}^*$. Then, we can express the equations in (15) in the same forms as those in (11) for the TZF/TRD-PSM, i.e.,

$$\begin{aligned} y_{m_1} &= \beta x + n_{m_1}, \\ y_m &= n_m, \ m = 0, 1, \ldots, M_1 - 1 \text{ and } m \neq m_1 \end{aligned} \tag{16}$$

where n_m for $m \neq m_1$ is an interference plus Gaussian noise signal, which is approximately Gaussian distributed with zero mean and a variance of $\sigma_I^2 = |\beta' \boldsymbol{h}_m^T (\boldsymbol{H}_1^* \boldsymbol{H}_1^T + M_1\sigma^2 \boldsymbol{I}_N)^{-1} \boldsymbol{h}_{m_1}^*|^2 + 1/\gamma_s$. By contrast, n_{m_1} is Gaussian distributed with the variance $\sigma^2 = 1/\gamma_s$, which is smaller than the variance of the other n_m's.

III. Detection Algorithms for TRD-PSM System

In this section, we introduce a range of detection algorithms by taking into account the detection reliability and detection complexity of TRD-PSM systems. Both joint maximum likelihood detection (JMLD) and successive MLD (SMLD) algorithms are considered. Furthermore, in order to attain a good trade-off between complexity and reliability, we propose a RTT-assisted MLD (RTT-MLD). Below we first consider the JMLD, which is capable of achieving the best performance at the highest complexity among the detectors considered in this paper.

A. Joint Maximum Likelihood Detection

In the general cases where different precoding algorithms may be used, a **JMLD** can be built based on (3), which jointly estimates m_1 and x by solving the optimization problem of

$$\begin{aligned} \langle \hat{m}_1, \hat{x} \rangle &= \arg \min_{m_1' \in \mathcal{M}_1, x' \in \mathcal{X}} \left\{ \left\| \boldsymbol{y} - \boldsymbol{H}^T \boldsymbol{p}_{m_1'} x' \right\|^2 \right\} \\ &= \arg \max_{m_1' \in \mathcal{M}_1, x' \in \mathcal{X}} \left\{ \Re\left\{ \boldsymbol{y}^H \boldsymbol{H}^T \boldsymbol{p}_{m_1'} x' \right\} - \frac{1}{2} \left\| \boldsymbol{H}^T \boldsymbol{p}_{m_1'} x' \right\|^2 \right\} \end{aligned} \tag{17}$$

Upon applying (5), (6), and the related matrices (vectors) to the above equation, we obtain

$$\begin{aligned} \langle \hat{m}_1, \hat{x} \rangle = \arg \max_{m_1' \in \mathcal{M}_1, x' \in \mathcal{X}} \Big\{ & \Re\left\{ \boldsymbol{y}_1^H \boldsymbol{H}_1^T \boldsymbol{p}_{m_1'} x' + \boldsymbol{y}_d^H \boldsymbol{H}_d^T \boldsymbol{p}_{m_1'} x' \right\} \\ & - \frac{1}{2} \left(\left\| \boldsymbol{H}_1^T \boldsymbol{p}_{m_1'} x' \right\|^2 + \left\| \boldsymbol{H}_d^T \boldsymbol{p}_{m_1'} x' \right\|^2 \right) \Big\} \end{aligned} \tag{18}$$

When the TZF/TRD-PSM or when the TMMSE/TRD-PSM with the residue interference approximated by Gaussian noise is employed, with the aid of (11) or of (16), we can simplify (18) to a **simplified JMLD**, described as

$$\begin{aligned} \langle \hat{m}_1, \hat{x} \rangle = \arg \max_{m_1' \in \mathcal{M}_1, x' \in \mathcal{X}} \Big\{ & \Re\left\{ \beta y_{m_1'}^* x' + \boldsymbol{y}_d^H \boldsymbol{H}_d^T \boldsymbol{p}_{m_1'} x' \right\} \\ & - \frac{1}{2} \left(|\beta x'|^2 + \left\| \boldsymbol{H}_d^T \boldsymbol{p}_{m_1'} x' \right\|^2 \right) \Big\} \end{aligned} \tag{19}$$

Equations (18) and (19) show that the diversity antennas are capable of enhancing the detection reliability by providing M_d orders of receive diversity, as shown explicitly by our further analysis in Section IV. From (18) we can derive that the complexity of the JMLD is $\mathcal{O}(2M_1M_2MN)$. When the TZF/TRD-PSM or TMMSE/TRD-PSM is employed, the complexity of the simplified JMLD of (19) is $\mathcal{O}(2M_1M_2(M_dN+1))$, which is lower than that of the JMLD, due to the fact of $M_d < M$.

B. Successive Maximum Likelihood Detection

The SMLD first detects the M_1-SSK symbol m_1 using noncoherent detection. After the detection of the M_1-SSK symbol, the receiver knows which receive antenna for the M_1-SSK is activated and, hence, knows which precoding vector in $\boldsymbol{P}$ is used for the precoding. With the aid of this knowledge, the M_2-APM symbol can then be detected using coherent detection.

First, in order to detect the M_1-SSK symbol m_1 without invoking any knowledge about x except knowing that it belongs to an M_2-APM constellation, we may follow the noncoherent detection principles in [41–44] and build from (19) a detector as

$$\hat{m}_1 = \arg \max_{m_1' \in \mathcal{M}_1} \left\{ \mathbb{E}_x \left[\Re \left\{ \beta y_{m_1'}^* x + \boldsymbol{y}_d^H \boldsymbol{H}_d^T \boldsymbol{p}_{m_1'} x \right\} - \frac{1}{2} \left(\|\beta x\|^2 + \left\| \boldsymbol{H}_d^T \boldsymbol{p}_{m_1'} x \right\|^2 \right) \right] \right\} \quad (20)$$

where $\mathbb{E}_x[\cdot]$ is the expectation operation with respect to x. After the simplification following the principles in [41–44], as well as using $\mathbb{E}_x[|x|^2] = 1$ and ignoring the β^2 term, we can obtain

$$\hat{m}_1 = \arg \max_{m_1' \in \mathcal{M}_1} \left\{ \left| \beta y_{m_1'}^* + \boldsymbol{y}_d^H \boldsymbol{H}_d^T \boldsymbol{p}_{m_1'} \right| - \frac{\left\| \boldsymbol{H}_d^T \boldsymbol{p}_{m_1'} \right\|^2}{2} \right\} \quad (21)$$

For convenience, the detector based on (21) for detection of m_1 is referred to as the **SMLD**.

Note that, when all the receive antennas are used only for PSM, i.e., when $M_1 = M$, the detector of (21) is reduced to

$$\hat{m}_1 = \arg \max_{m_1' \in \mathcal{M}_1} \left\{ \left| y_{m_1'} \right| \right\} \quad (22)$$

Furthermore, even in the more general case of $M > M_1$, instead of using (21), in some references on SM, e.g., [10, 15], the simplified detector of

$$\hat{m}_1 = \arg \max_{m_1' \in \mathcal{M}_1} \left\{ \left| \beta y_{m_1'}^* + \boldsymbol{y}_d^H \boldsymbol{H}_d^T \boldsymbol{p}_{m_1'} \right| \right\} \quad (23)$$

is usually used. For distinction, we refer to the SMLD using (23) for detection of m_1 as the **simplified SMLD**.

Comparing (21) and (23), the SMLD has an extra term of $\|\boldsymbol{H}_d^T \boldsymbol{p}_{m_1'}\|^2/2$. The value of this term can be very different for applying different precoding vectors $\boldsymbol{p}_{m_1'}$. Consequently, ignoring it generates interference on the detection and may significantly degrade the achievable performance. However, when N and M_d are very large, it is expected that $\|\boldsymbol{H}_d^T \boldsymbol{p}_{m_1'}\|^2$ converges to a constant[2]. In this case, the SMLD of (21) converges the simplified SMLD of (23). In Section V, we will compare the performance achieved by (21) and (23), to show that the error performance achieved by the detector of (23) is in general worse than that achieved by the detector of (21).

After the detection of the M_1-SSK symbol m_1 using either (21) or (23), from (5) and (6) we can obtain the observations of

$$\begin{aligned} y_{\hat{m}_1} &= \beta \delta(\hat{m}_1, m_1) x + n_{\hat{m}_1} \\ \boldsymbol{y}_d &= \boldsymbol{H}_d^T \boldsymbol{p}_{m_1} x + \boldsymbol{n}_d \end{aligned} \quad (24)$$

where $\delta(m_1, m_1) = 1$ and $\delta(\hat{m}_1, m_1) = 0$, when $\hat{m}_1 \neq m_1$. Since at this stage the receiver assumes that the transmitted M_1-SSK symbol is $\hat{m}_1$, it can use the maximum ratio combining (MRC), which is optimum, to form the decision variable as

$$X = \beta y_{\hat{m}_1} + \boldsymbol{p}_{\hat{m}_1}^H \boldsymbol{H}_d^* \boldsymbol{y}_d \quad (25)$$

for detection of the M_2-APM symbol x. Based on this equation, if m_1 was correctly detected, i.e., if $\hat{m}_1 = m_1$, then, X is given by

$$X = \left(\beta^2 + \|\boldsymbol{H}_d^T \boldsymbol{p}_{m_1}\|^2 \right) x + n \quad (26)$$

where $n = \beta n_{m_1} + \boldsymbol{p}_{m_1}^H \boldsymbol{H}_d^* \boldsymbol{n}_d$. Therefore, x can be detected with $(M_d + 1)$ orders of diversity, rendering the detection very reliable, if M_d is relatively large. By contrast, if m_1 was erroneously detected, i.e., when $\hat{m}_1 \neq m_1$, then, X is given by

$$X = \left(\boldsymbol{p}_{\hat{m}_1}^H \boldsymbol{H}_d^* \boldsymbol{H}_d^T \boldsymbol{p}_{m_1} \right) x + n \quad (27)$$

where $n = \beta n_{\hat{m}_1} + \boldsymbol{p}_{\hat{m}_1}^H \boldsymbol{H}_d^* \boldsymbol{n}_d$, while the amplitude in the front of x is a complex random variable. In this case, the detection of x is equivalent to a random guess, and the probability of correct detection is about $1/M_2$.

Therefore, for both the SMLD and the simplified SMLD, reliable detection of the M_1-SSK symbol is critical, which dominates the reliability of the whole PSM system. Unfortunately, in the above described SMLDs, the M_1-SSK symbol m_1 is noncoherently detected. In comparison to the JMLD, the detection reliability of the SMLDs should be much lower. However, both the SMLDs have much lower complexity than the JMLD. Specifically, the complexity of the SMLD can be readily analyzed from (21) and (25), which is $\mathcal{O}(M_1 + 2M_1M_dN + M_dN + M_2)$, where the first two terms are contributed by the detection of M_1-SSK symbol, while the other two by the detection of the M_2-APM symbol. In the bracket, the term of NM_dM_1 is for computing $\boldsymbol{H}_d^T \boldsymbol{p}_{m_1'}$ in (21), computing all the other terms in (21) has lower number of operations than computing this one. M_1 is added for the case $M_d = 0$, while M_2 takes into account of the complexity for the M_2-APM demodulation based on (26). In the next section, we propose a ratio threshold test assisted MLD (RTT-MLD), in order to attain an error performance significantly better than that of the SMLD, but with a detection complexity much lower than that of the JMLD.

[2]When $N \to \infty$ and $M_d \to \infty$, by following the law of large numbers, we have $\boldsymbol{H}_1^T \boldsymbol{H}_1^* \to N \boldsymbol{I}_{M_1}$ and $\boldsymbol{H}_d^* \boldsymbol{H}_d^T \to M_d \boldsymbol{I}_N$. Therefore, we can derive that $\|\boldsymbol{H}_d^T \boldsymbol{p}_{m_1'}\|^2 \to M_d \boldsymbol{e}_{m_1'}^T \boldsymbol{H}_1^T \boldsymbol{H}_1^* \boldsymbol{e}_{m_1'}/N \to M_d$.

C. Ratio Threshold Test Aided Maximum Likelihood Detection

Based on (21), let us express the M_1 decision variables given for detection of the M_1-SSK symbol as

$$Y_i = \left|\beta y_i^* + \boldsymbol{y}_d^H \boldsymbol{H}_d^T \boldsymbol{p}_i\right| - \frac{\left\|\boldsymbol{H}_d^T \boldsymbol{p}_i\right\|^2}{2},\ i = 0, 1, \ldots, M_1 - 1 \tag{28}$$

Based on (22), we may build an even simpler scheme based on the decision variables of

$$Y_i = \left|y_i\right|^2,\ i = 0, 1, \ldots, M_1 - 1 \tag{29}$$

In principle, we can use the M_1 decision variables either in (28) or in (29) to estimate the received M_1-SSK symbol. Let us reorder Y_i in descending order as

$$Y_{d_0}, Y_{d_1}, \ldots, Y_{d_{M_1-1}} \tag{30}$$

where $Y_{d_i} \geq Y_{d_{i+1}}$ and $d_i \in \mathcal{M}_1$. Let us express the ratio between the second maximum and the maximum of the M_1 variables given in (28) or (29) as

$$R = Y_{d_1}/Y_{d_0} \tag{31}$$

Then, according to the principles of the RTT [36–39], when conditioned on that the M_1-SSK symbol is correctly detected, R usually has a small value distributed close to zero. By contrast, when conditioned on that the M_1-SSK symbol is erroneously detected, R usually has a relatively large value distributed close to one. As some examples, based on (28), Fig. 1 plots the distributions of R, when given the M_1-SSK symbols correctly or erroneously detected, and when the TZF and TMMSE are respectively employed. Explicitly, when the M_1-SSK symbols are correctly detected, R is mainly distributed close to zero. By contrast, when the M_1-SSK symbols are erroneously detected, R is distributed in the region towards one. This behavior becomes more declared, as the SNR γ_b increases.

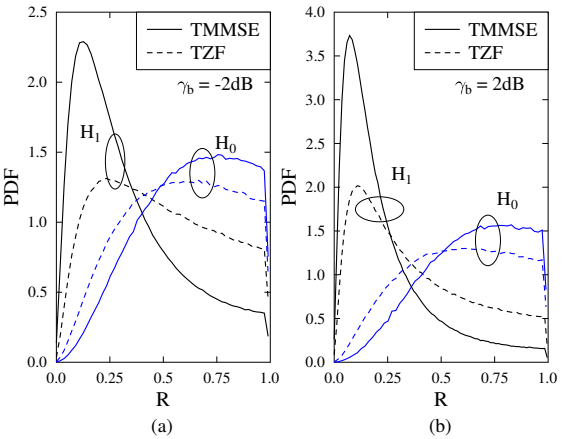

Fig. 1. PDFs of R conditioned on that the M_1-SSK symbols are correctly detected (H_1) or erroneously detected (H_0), when assuming that $N = 4$, $M = 6$, 4SSK, Quadrature Phase-Shift Keying (QPSK), and $\gamma_b = -2$dB (a), $\gamma_b = 2$dB (b).

Therefore, in the RTT-MLD, we can use the RTT to first test whether the detection of a M_1-SSK symbol is reliable. For this purpose, let T_h be a threshold, which can be set offline according to the reliability requirement. Then, if the corresponding R is lower than T_h, we render the detection of the M_1-SSK symbol reliable. In this case, the RTT-MLD forwards to detect the M_2-APM symbol. Otherwise, when the corresponding R is higher than T_h, meaning that the detection of the M_1-SSK symbol is not confidently reliable, we then form from (30) a subset having M_h elements, which is expressed as $\mathcal{D} = \{d_0, d_1, \ldots, d_{M_h-1}\}$. Based on this subset, the M_1-SSK and M_2-APM symbols are detected by solving the optimization problem of

$$\langle \hat{m}_1, \hat{x} \rangle = \arg \max_{m_1' \in \mathcal{D}, x' \in \mathcal{X}} \left\{ \Re \left\{ \beta y_{m_1'}^* x' + \boldsymbol{y}_d^H \boldsymbol{H}_d^T \boldsymbol{p}_{m_1'} x' \right\} - \frac{1}{2} \left(\left|\beta x'\right|^2 + \left\|\boldsymbol{H}_d^T \boldsymbol{p}_{m_1'} x'\right\|^2 \right) \right\} \tag{32}$$

which is the same as (19), but has a search space determined by $\mathcal{D}$ instead of $\mathcal{M}_1$.

According to [36–39], we can be implied that, when a M_1-SSK symbol is detected in error, the second or the third largest in $\{Y_i\}$ of (30) is most probably the correct one. Based on this fact, in the RTT-MLD, the size M_h of $\mathcal{D}$ is usually very small, typically, less than five. Hence, the complexity of the RTT-MLD can be significantly lower than that of the simplified JMLD described in Section III-A.

To support the above argument, Fig. 2 depicts the impact of M_h on the BER performance of the RTT-MLD associated with $T_h = 0.1$. For the sake of comparison, in the figure, the BER performance of the PSM systems with the simplified JMLD is also provided. As shown in Fig. 2, as M_h is increased from 1 to 4, the BER performance of the RTT-MLD becomes closer and closer to that of the simplified JMLD. Furthermore, in contrast to the significant performance improvement, when increasing M_h from 1 to 2, slight performance improvement is observed, when increasing M_h from 3 to 4. Therefore, in practice, using a relatively small value of M_h can guarantee that most of performance gain is attained, but at much lower detection complexity.

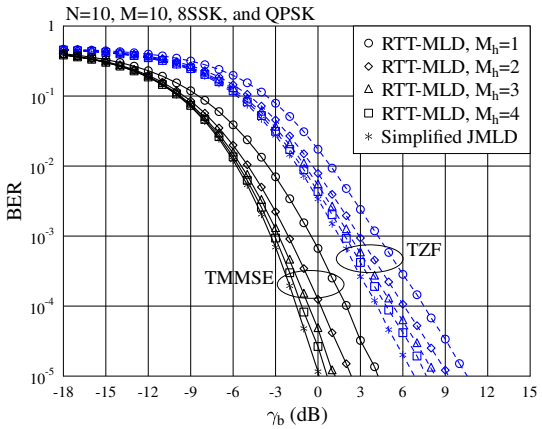

Fig. 2. BER versus average SNR per bit performance of the TRD-PSM systems employing, respectively, the simplified JMLD (19) and RTT-MLD (32), when assuming $N = 10$, $M = 10$, 8SSK, and QPSK.

Finally, after ignoring the less significant terms contributing to the complexity and for the convenience of comparison, the complexity of the different detectors provided in this

TABLE I
COMPLEXITY OF THE VARIOUS DETECTORS

Detector	Complexity
JMLD	$\mathcal{O}(2M_1M_2MN)$
Simplified JMLD	$\mathcal{O}(2M_1M_2M_dN)$
SMLD	$\mathcal{O}(2M_1M_dN)$
Simplified SMLD	$\mathcal{O}(M_1M_dN)$
RTT-MLD	$\mathcal{O}(2M_1M_dN)$

section is summarized in Table I. Explicitly, the JMLD has the highest complexity, while the simplified SMLD has the lowest complexity. The RTT-MLD has a similar complexity as the SMLD.

IV. PERFORMANCE ANALYSIS OF TRD-PSM SYSTEMS

In this section, we analyze the ABEP of TRD-PSM systems, when the JMLD or simplified JMLD introduced in Section III is employed. The reason for us to consider in particular these two representative detectors is that, first, the optimum JMLD provides a performance upper-bound for all the detectors considered. Second, the simplified JMLD can provide a close approximation for the performance of the RTT-MLD, and also for that of the SMLD employing a relatively big number of diversity antennas. Below we first analyze the TRD-PSM systems employing the JMLD described by (18). The analytical results are then modified for the TRD-PSM systems with the simplified JMLD defined by (19). Our analysis will address two cases. In the first case, we derive a union-bound for the ABEP of the small-scale TRD-PSM systems. By contrast, the second case considers the large-scale TRD-PSM systems, and we analyze the asymptotic ABEP of TRD-PSM systems.

A. ABEP of TRD-PSM Systems with JMLD

1) Small-Scale TRD-PSM Systems: For small-scale TRD-PSM systems, we assume that $N > M_1$ and N takes a relatively small value. Upon adopting the union-bound approach [44], we can obtain that the ABEP of the PSM systems employing the JMLD of (18) satisfies

$$P_e \leq \frac{1}{k_b 2^{k_b}} \sum_{\langle m_1,x\rangle} \sum_{\langle m_1',x'\rangle} d_H\left(\langle m_1,x\rangle, \langle m_1',x'\rangle\right) \mathbb{E}_{\boldsymbol{H}}\left[\text{PEP}\left\{\langle m_1,x\rangle \to \langle m_1',x'\rangle\right\}\right] \tag{33}$$

where $k_b = k_1 + k_2$, $d_H(x,y)$ is the Hamming distance between the two binary-represented symbols x and y, and $\mathbb{E}_{\boldsymbol{H}}[\text{PEP}\{\langle m_1,x\rangle \to \langle m_1',x'\rangle\}]$ denotes the average pairwise error probability (APEP) after averaging with respect to the related channels. With the aid of (18), the pairwise error probability (PEP) of receiving $\langle m_1',x'\rangle$ given that $\langle m_1,x\rangle$ was transmitted can be formulated as

$$\begin{aligned}
&\text{PEP}\left\{\langle m_1,x\rangle \to \langle m_1',x'\rangle\right\} \\
&= P_r\left\{2\Re\left\{\boldsymbol{y}^H\left(\boldsymbol{H}^T\boldsymbol{p}_{m_1'}x' - \boldsymbol{H}^T\boldsymbol{p}_{m_1}x\right)\right\} > \left\|\boldsymbol{H}^T\boldsymbol{p}_{m_1'}x'\right\|^2 - \left\|\boldsymbol{H}^T\boldsymbol{p}_{m_1}x\right\|^2\right\} \\
&= P_r\left\{2\Re\left\{\left(\boldsymbol{H}^T\boldsymbol{p}_{m_1'}x' - \boldsymbol{H}^T\boldsymbol{p}_{m_1}x\right)^H\boldsymbol{n}\right\} > \left\|\boldsymbol{H}^T\boldsymbol{p}_{m_1'}x' - \boldsymbol{H}^T\boldsymbol{p}_{m_1}x\right\|^2\right\} \\
&= Q\left(\sqrt{\frac{v+w}{2\sigma^2}}\right)
\end{aligned} \tag{34}$$

where $Q(\cdot)$ is the well-known Gaussian Q-function [45], $v = \|\boldsymbol{H}_1^T(\boldsymbol{p}_{m_1'}x' - \boldsymbol{p}_{m_1}x)\|^2$, and $w = \|\boldsymbol{H}_d^T(\boldsymbol{p}_{m_1'}x' - \boldsymbol{p}_{m_1}x)\|^2$.

In order to obtain the relatively simple expressions that are convenient to evaluate, we introduce a tight upper-bound for the Q-function [45], given by $Q(x) \leq \exp(-2x^2)/6 + \exp(-x^2)/12 + \exp(-x^2/2)/4$. Then, we can express the PEP of (34) as

$$\text{PEP}\left\{\langle m_1,x\rangle \to \langle m_1',x'\rangle\right\} \leq \sum_{j=1}^{3} \tau_j \exp\left(-\frac{v+w}{\alpha_j}\right) \tag{35}$$

where $\tau_1 = \frac{1}{6}$, $\tau_2 = \frac{1}{12}$, and $\tau_3 = \frac{1}{4}$, while $\alpha_1 = \sigma^2$, $\alpha_2 = 2\sigma^2$, and $\alpha_3 = 4\sigma^2$. Therefore, when substituting (35) into (33), we have

$$P_e \leq \frac{1}{k_b 2^{k_b}} \sum_{\langle m_1,x\rangle} \sum_{\langle m_1',x'\rangle} d_H\left(\langle m_1,x\rangle, \langle m_1',x'\rangle\right) \mathbb{E}_{\boldsymbol{H}}\left[g\left(v,w\right)\right] \tag{36}$$

where, by definition, $g(v,w) = \sum_{j=1}^{3} \tau_j e^{-(v+w)/\alpha_j}$, the average of which in terms of $\boldsymbol{H}$ is analyzed as follows.

Following the moment generating function (MGF) approach [44], we can express the expectation in (36) as

$$\begin{aligned}
\mathbb{E}_{\boldsymbol{H}}\left[g\left(v,w\right)\right] &= \mathbb{E}_{\boldsymbol{H}_1}\left[\sum_{j=1}^{3}\tau_j \exp\left(-\frac{v}{\alpha_j}\right)\mathbb{E}_{\boldsymbol{H}_d}\left[\exp\left(-\frac{w}{\alpha_j}\right)\right]\right] \\
&= \mathbb{E}_{\boldsymbol{H}_1}\left[\sum_{j=1}^{3}\tau_j \exp\left(-\frac{v}{\alpha_j}\right)\mathcal{M}_w\left(-\frac{w}{\alpha_j}\right)\right] \\
&= \mathbb{E}_{\boldsymbol{H}_1}\left[\sum_{j=1}^{3}\tau_j \exp\left(-\frac{v}{\alpha_j}\right)\left(\frac{\alpha_j}{\left\|\boldsymbol{p}_{m_1'}x' - \boldsymbol{p}_{m_1}x\right\|^2 + \alpha_j}\right)^{M_d}\right]
\end{aligned} \tag{37}$$

where $\mathcal{M}_w(\cdot)$ is the MGF of w, and the last equation is due to the assumption of independent identically distributed (iid) Rayleigh fading [46].

Remark 1: When the average SNR per symbol γ_s is high, making $\sigma^2 = 1/\gamma_s \to 0$, using the values of α_j, we can simplify the expectation in (37) to

$$\mathbb{E}_{\boldsymbol{H}}\left[g\left(v,w\right)\right] = \mathbb{E}_{\boldsymbol{H}_1}\left[\frac{\sum_{j=1}^{3}\tau_j c_j^{M_d}\exp\left(-\frac{v}{\alpha_j}\right)}{\left\|\boldsymbol{p}_{m_1'}x' - \boldsymbol{p}_{m_1}x\right\|^{-2M_d}}\right]\gamma_s{}^{-M_d} \tag{38}$$

where $c_1 = 1$, $c_2 = 2$ and $c_3 = 4$. In (38), the term of ${\gamma_s}^{-M_d}$ explains that the employment of M_d diversity antennas results in M_d orders of receive diversity.

To this point, further simplifying (38) becomes very hard, even when the TZF and TMMSE precoders are considered. Specifically, when the TZF precoder is employed, we can have $v = \beta^2 \|\boldsymbol{e}_{m_1'} x' - \boldsymbol{e}_{m_1} x\|^2$. Then, the problem can be modified to derive the probability density function (PDF) of β, which is still hard to obtain a closed-form expression, as β has a complicated structure of $\boldsymbol{H}_1$ [27]. The situation becomes even worse when the TMMSE precoder is employed, as in this case v is more complicated than that in the TZF case. Therefore, in the case of finite N, we approximate $\eta = v + w$ as a Gamma distributed random variable, i.e., Gamma-approximation (Gamma-Ap)[3] [48]. As shown in Section V of this paper, the Gamma-Ap is highly effective for performance evaluation.

With the aid of the Gamma-Ap, we approximate η as the Gamma distributed random variable with a PDF [47] of

$$f(\eta) = \frac{\eta^{m_\eta - 1}}{\Gamma(m_\eta)} (\Omega_\eta)^{-m_\eta} e^{-\eta/\Omega_\eta}, \ \eta \geq 0 \tag{39}$$

whose distribution parameters m_η and Ω_η are given by

$$\begin{aligned} m_\eta &= (\mathbb{E}[\eta])^2 / \mathbb{E}\left[(\eta - \mathbb{E}[\eta])^2\right] \\ \Omega_\eta &= \mathbb{E}\left[(\eta - \mathbb{E}[\eta])^2\right] / \mathbb{E}[\eta] \end{aligned} \tag{40}$$

Explicitly, m_η and Ω_η are functions of v and w, which are hard to obtain analytical solutions. However, their values can be readily obtained via numerical simulations. As shown in [48], about 10^4 channel realizations are usually sufficient for obtaining reliable estimations of m_η and Ω_η. Therefore, in our following studies, we use 10^4 Monte-Carlo simulations to estimate the parameters of the Gamma PDF of (39).

With the aid of the Gamma-Ap of η, we can then have the following Theorem for simplifying the expectation in (34).

Theorem 1: Given the Gamma PDF of η as shown in (39), the expectation in (34) can be expressed as

$$\begin{aligned} \mathbb{E}_{\boldsymbol{H}}[g(v,w)] &= \int_0^\infty g(\eta) f(\eta) d\eta \\ &= \sum_{j=1}^{3} \tau_j \left(\frac{\alpha_j}{\Omega_\eta + \alpha_j}\right)^{m_\eta} \end{aligned} \tag{41}$$

Proof: See Appendix A. ∎

Upon substituting (41) into (34), the approximate ABEP upper-bound can be given by the following corollary.

Corollary 1: When the Gamma-Ap for $\eta = v + w$ is used, an approximate ABEP upper-bound for the TRD-PSM system with JMLD is

$$P_e^{ub,app} = \frac{1}{k_b 2^{k_b}} \sum_{\langle m_1, x\rangle} \sum_{\langle m_1', x'\rangle} d_H(\langle m_1, x\rangle, \langle m_1', x'\rangle) \sum_{j=1}^{3} \tau_j \left(\frac{\alpha_j}{\Omega_\eta + \alpha_j}\right)^{m_\eta}. \tag{42}$$

[3]Note that, the sensibility of using the Gamma-Ap is that, no matter TZF or TMMSE is employed, $\boldsymbol{H}^T \boldsymbol{p}_{m_1'} x'$ and $\boldsymbol{H}^T \boldsymbol{p}_{m_1} x$ in (34) are near-Gaussian distributed, and hence, $\eta = v + w$ is near-Gamma distributed [44, 47].

Let us below consider the large-scale TRD-PSM systems.

2) Large-Scale TRD-PSM Systems: In the large-scale TRD-PSM systems, we assume that $N >> M_1$. Then, according to the principles of massive MIMO [49], both the TZF and TMMSE converge to the transmit matched-filtering (TMF) based precoding, which is also optimum in the sense of maximum SNR. Therefore, the optimum precoding matrix is

$$\boldsymbol{P} = \boldsymbol{H}_1^* / \sqrt{N} \tag{43}$$

Correspondingly, v and w in (34) can be expressed as

$$v = N \left\|\boldsymbol{e}_{m_1'} x' - \boldsymbol{e}_{m_1} x\right\|^2 \tag{44}$$

$$w = \left\|\boldsymbol{H}_d^T \boldsymbol{u}\right\|^2 \tag{45}$$

where $\boldsymbol{u} = \boldsymbol{H}_1^* (\boldsymbol{e}_{m_1'} x' - \boldsymbol{e}_{m_1} x)/\sqrt{N}$. Consequently, $g(v,w)$ in (36) can be expressed as

$$g(v,w) = \sum_{j=1}^{3} \tau_j \exp\left(-\frac{N d_{mx} + \left\|\boldsymbol{H}_d^T \boldsymbol{u}\right\|^2}{\alpha_j}\right) \tag{46}$$

where $d_{mx} = \|\boldsymbol{e}_{m_1'} x' - \boldsymbol{e}_{m_1} x\|^2$. Furthermore, as $\boldsymbol{H}_1$ and $\boldsymbol{H}_d$ are independent, the expectation on (46) can be obtained by first averaging it over $\boldsymbol{H}_d$, and then averaging the result over $\boldsymbol{H}_1$, which is expressed as

$$\begin{aligned} \mathbb{E}_{\boldsymbol{H}}[g(v,w)] = &\sum_{j=1}^{3} \tau_j \exp\left(-\frac{N d_{mx}}{\alpha_j}\right) \\ &\mathbb{E}_{\boldsymbol{H}_1}\left[\mathbb{E}_{\boldsymbol{H}_d}\left[\exp\left(-\frac{\left\|\boldsymbol{H}_d^T \boldsymbol{u}\right\|^2}{\alpha_j}\right)\right]\right] \end{aligned} \tag{47}$$

After the simplification, we have $\mathbb{E}_{\boldsymbol{H}}\{g(v,w)\}$ as summarized by the following theorem.

Theorem 2: In the large-scale TRD-PSM systems satisfying $N >> M_1$, $\mathbb{E}_{\boldsymbol{H}}[g(v,w)]$ is given by

$$\mathbb{E}_{\boldsymbol{H}}[g(v,w)] \approx \sum_{j=1}^{3} \tau_j \exp\left(-\frac{N d_{mx}}{\alpha_j}\right) \left(\frac{\alpha_j}{d_{mx} + \alpha_j}\right)^{M_d} \tag{48}$$

Proof: See Appendix B. ∎

Furthermore, when substituting (48) into (36), we have the following corollary for an ABEP upper-bound.

Corollary 2: An asymptotic ABEP upper-bound for a large-scale TRD-PSM system with $N >> M_1$ can be formulated as

$$\begin{aligned} P_e^{ub,asy} = &\frac{1}{k_b 2^{k_b}} \sum_{\langle m_1, x\rangle} \sum_{\langle m_1', x'\rangle} d_H(\langle m_1, x\rangle, \langle m_1', x'\rangle) \\ &\sum_{j=1}^{3} \tau_j \exp\left(-\frac{N d_{mx}}{\alpha_j}\right) \left(\frac{\alpha_j}{d_{mx} + \alpha_j}\right)^{M_d} \end{aligned} \tag{49}$$

Remark 2: In the high SNR region of $\sigma^2 \to 0$, (49) can be further approximated as

$$\begin{aligned} P_e^{ub,asy} \approx &\frac{1}{k_b 2^{k_b}} \sum_{\langle m_1, x\rangle} \sum_{\langle m_1', x'\rangle} d_H(\langle m_1, x\rangle, \langle m_1', x'\rangle) \\ &\sum_{j=1}^{3} \frac{\tau_j c_j^{M_d}}{d_{mx}^{M_d}} \exp\left(-\frac{N d_{mx}}{\alpha_j}\right) {\gamma_s}^{-M_d} \end{aligned} \tag{50}$$

where $c_1 = 1$, $c_2 = 2$ and $c_3 = 4$. From (50) we are also implied that, in the TRD-PSM systems employing M_d diversity antennas, M_d extra orders of diversity are achievable.

B. ABEP of TRD-PSM Systems with Simplified JMLD

Above we have analyzed the ABEP of the TRD-PSM systems with the JMLD described by (18). Below we extend our analysis to the TRD-PSM systems with the simplified JMLD of (19). In these cases, from (11) for the TZF/TRD-PSM and (16) for the TMMSE/TRD-PSM, we can express the PEP as

$$\begin{aligned}&\text{PEP}\left\{\langle m_1, x\rangle, \langle m_1', x'\rangle\right\}\\&= P_r\Big\{2\Re\left\{\beta \boldsymbol{y}_1^H \boldsymbol{e}_{m_1'} x' + \boldsymbol{y}_d^H \boldsymbol{H}_d^T \boldsymbol{p}_{m_1'} x'\right\} - \left\|\beta \boldsymbol{e}_{m_1'} x'\right\|^2\\&\qquad - \left\|\boldsymbol{H}_d^T \boldsymbol{p}_{m_1'} x'\right\|^2 > 2\Re\left\{\beta \boldsymbol{y}_1^H \boldsymbol{e}_{m_1} x + \boldsymbol{y}_d^H \boldsymbol{H}_d^T \boldsymbol{p}_{m_1} x\right\}\\&\qquad -\|\beta \boldsymbol{e}_{m_1} x\|^2 - \left\|\boldsymbol{H}_d^T \boldsymbol{p}_{m_1} x\right\|^2\Big\} \quad (51)\end{aligned}$$

Specifically, when the TZF/TRD-PSM is considered, it can be shown that in (34), after expanding $\boldsymbol{H}^T \boldsymbol{p}_{m_1}$ and $\boldsymbol{H}^T \boldsymbol{p}_{m_1'}$, and making use of $\boldsymbol{H}_1^T \boldsymbol{p}_{m_1} = \boldsymbol{e}_{m_1}$ and $\boldsymbol{H}_1^T \boldsymbol{p}_{m_1'} = \boldsymbol{e}_{m_1'}$, it gives the same expression of (51). Therefore, the TZF/TRD-PSM employing the simplified JMLD achieves the same error performance as the TZF/TRD-PSM employing the JMLD. In other words, when the TZF/TRD-PSM employing the simplified JMLD of (19), the corresponding PEP can be evaluated by the same approach in Sections IV-A1 and IV-A2.

When the TMMSE/TRD-PSM is employed, using (16), we can further simplify (51) to

$$\begin{aligned}&\text{PEP}\left\{\langle m_1, x\rangle, \langle m_1', x'\rangle\right\}\\&= P_r\Big\{2\Re\Big\{n_{m_1'}^* \beta\left(m_1'\right) x' - n_{m_1}^* \beta\left(m_1\right) x + \boldsymbol{n}_d^H \boldsymbol{H}_d^T\\&\qquad \left(\boldsymbol{p}_{m_1'} x' - \boldsymbol{p}_{m_1} x\right)\Big\} > \left|\beta\left(m_1'\right) x'\right|^2 + \left|\beta\left(m_1\right) x\right|^2\\&\qquad +\left\|\boldsymbol{H}_d^T\left(\boldsymbol{p}_{m_1'} x' - \boldsymbol{p}_{m_1} x\right)\right\|^2\Big\}\\&= Q\left(\delta/\sqrt{2\xi}\right), \quad (52)\end{aligned}$$

where $\beta(m_1) = \beta' \boldsymbol{h}_{m_1}^T (\boldsymbol{H}_1^* \boldsymbol{H}_1^T + M_1 \sigma^2 \boldsymbol{I}_N)^{-1} \boldsymbol{h}_{m_1}^*$, $\delta = \|\beta(m_1') \boldsymbol{e}_{m_1'} x' - \beta(m_1) \boldsymbol{e}_{m_1} x)\|^2 + \|\boldsymbol{H}_d^T (\boldsymbol{p}_{m_1'} x' - \boldsymbol{p}_{m_1} x)\|^2$, and

$$\xi = \begin{cases} \delta\sigma^2, & m_1' = m_1 \\ |\beta(m_1')x'|^2\sigma_I^2 + |\beta(m_1)x|^2\sigma^2 & \\ \quad + \|\boldsymbol{H}_d^T(\boldsymbol{p}_{m_1'} x' - \boldsymbol{p}_{m_1} x)\|^2\sigma^2, & m_1' \neq m_1 \end{cases} \quad (53)$$

As shown in (52), for a limited value of N, the PEP of TMMSE/TRD-PSM systems has a very complicated structure of the related channels, which makes the simplification and further derivation of a closed-form expression for the ABEP upper-bound highly involved. However, it is well-known that the TMMSE precoder always slightly outperforms the TZF precoder and, when SNR is sufficiently high, both of them attain a similar error performance. Therefore, in this paper, we do not attempt to further simplify the PEP of (52).

When comparing (34) and (52), we can know that the error performance achieved by the TMMSE/TRD-PSM systems with simplified JMLD should be worse than that of the TMMSE/TRD-PSM systems with JMLD, due to the factor that ξ in (52) is larger than σ^2. This is because the JMLD can make use of the 'interference' generated by the TMMSE precoder for performance improvement, while the simplified JMLD treats this interference as Gaussian noise.

Note furthermore that, in the case of $N \to \infty$, as shown in Section IV-A2, the TMMSE, TZF as well as the TMF precoders are all optimum. Hence, the simplified JMLD achieves the same error performance as the JMLD. Consequently, the expression of (49) also provides an asymptotic ABEP upper-bound for both the TMMSE/TRD-PSM and TZF/TRD-PSM systems employing the simplified JMLD.

V. Performance Results and Discussion

In this section, we will demonstrate and compare the error performance of the TRD-PSM systems employing TZF or TMMSE, associated with various detection algorithms, including the JMLD, simplified JMLD, SMLD, simplified SMLD, and the RTT-MLD, respectively. The statements made in Section III and Section IV will be validated. Furthermore, we will validate the approximate and asymptotic ABEP upper-bounds derived in Section IV by the Monte-Carlo simulations. Additionally, we will compare the error performance between the TRD-PSM systems providing receive diversity with that of the conventional pure PSM systems, where all receive antennas are used for SSK modulation. Note that, in the following figures, when the RTT-MLD of (32) is considered, we set $M_h = 4$ and $T_h = 0.1$, which are the desired values obtained from our tests.

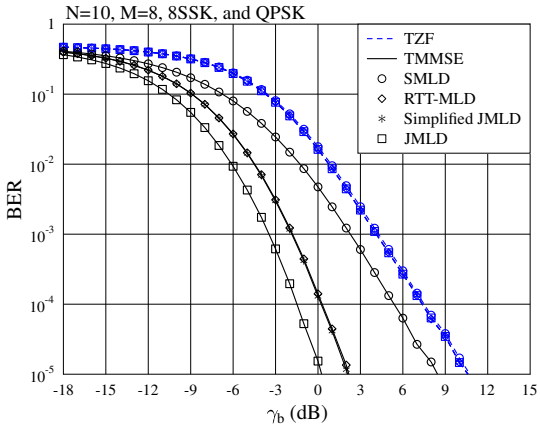

Fig. 3. BER versus average SNR per bit performance of the pure PSM systems with various precoding and detection schemes.

First, let us demonstrate the BER performance of the pure PSM systems ($M_d = 0$) in Fig. 3, when the precoders of TZF and TMMSE, as well as various detectors are respectively employed. The parameters used in our simulations are detailed on the top of the figure, the same are in the following figures. Note that, when $M_d = 0$, both the SMLD and simplified SMLD become the same. From the results shown in Fig. 3, we may have the following observations. First, as illustrated in Fig. 3 as well as in the following figures, TMMSE always outperforms TZF in term of the BER performance. Second, when TZF is employed, all the detectors achieve the same BER performance. This is because, when TZF is employed,

the JMLD, simplified JMLD and the RTT-MLD are actually the same in the case of $M_d = 0$, which slightly outperform the SMLD in terms of the BER performance. Third, when TMMSE is employed, the JMLD yields the best BER performance. In comparison to the JMLD, the SMLD has a big performance loss, which requires about 8 dB of extra transmit power than the JMLD at 10^{-5}. As seen in Fig. 3, both the simplified JMLD and the RTT-MLD, which attain nearly the same BER performance, have about 2 dB SNR loss at the 10^{-5} BER, when in comparison with the JMLD. However, both of them significantly outperform the SMLD.

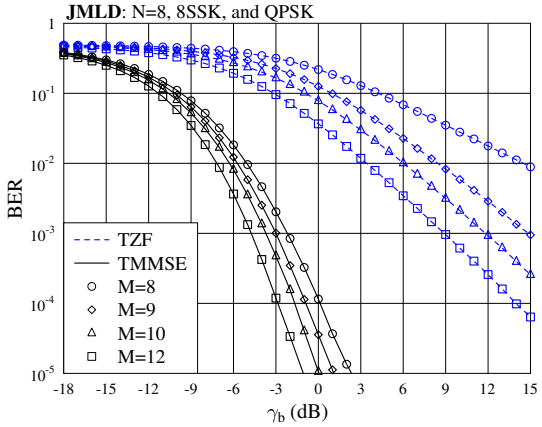

Fig. 4. BER versus average SNR per bit performance of the TRD-PSM systems with JMLD of (18).

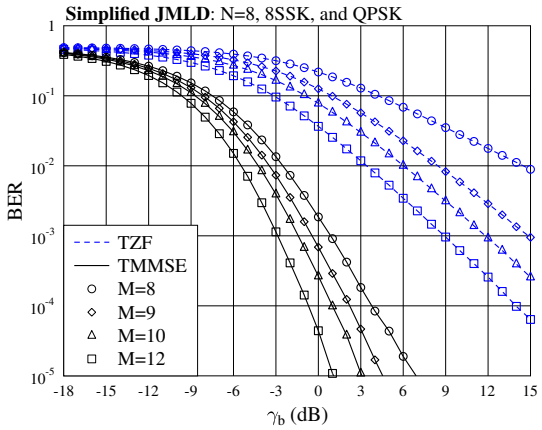

Fig. 5. BER versus average SNR per bit performance of the TRD-PSM systems with simplified JMLD of (19).

In Figs. 4-8, we characterize the BER performance of the TRD-PSM systems, when the JMLD (Fig. 4), simplified JMLD (Fig. 5), RTT-MLD (Fig. 6), SMLD (Fig. 7), and the simplified SMLD (Fig. 8) are respectively employed. As shown in the figures, we assume $N = 8$ and $M_1 = 8$ for 8SSK. Hence, $M = 8,\ 9,\ 10,\ 12$ correspond to $M_d = 0,\ 1,\ 2,\ 4$, respectively. Figs. 4-7 explicitly show that diversity gain is available, as the number of diversity antennas, i.e., M_d, increases. To be more specific, as shown in Figs. 4 and 5, for the TZF/TRD-PSM systems employing the JMLD or simplified JMLD, significant diversity gain is observed, when M_d is increased from 0 to 4. By contrast, when the TZF/TRD-PSM systems employ the RTT-MLD or SMLD, as shown in Figs. 6 and 7, a lower diversity gain than that in Figs. 4 and

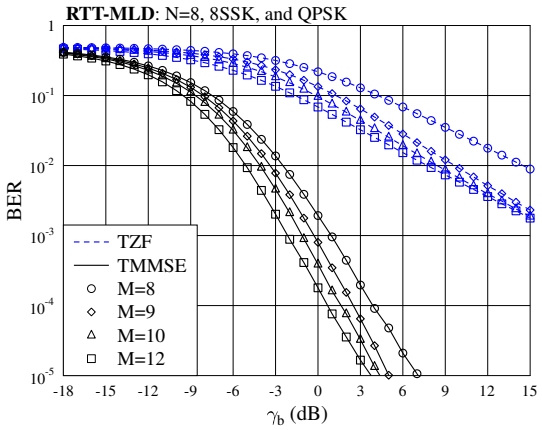

Fig. 6. BER versus average SNR per bit performance of the TRD-PSM systems with RTT-MLD of (32), when $M_h = 4$ and $T_h = 0.1$.

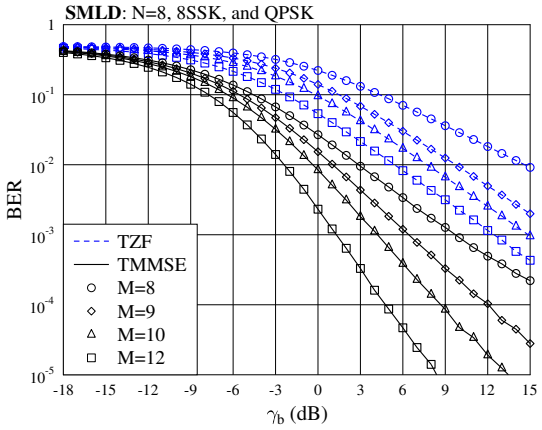

Fig. 7. BER versus average SNR per bit performance of the TRD-PSM systems with SMLD of (21) and (26).

5 is observed. On the other hand, when the TMMSE/TRD-PSM systems are considered, as shown in Figs. 4–7, the largest diversity gain is provided by the SMLD, although the JMLD, simplified JMLD and the RTT-MLD employed in Fig. 4, Fig. 5 and Fig. 6 outperform the SMLD. When comparing the BER performance demonstrated in Figs. 4-7, we observe that for the TMMSE/TRD-PSM systems, the simplified JMLD only slightly outperforms the RTT-MLD, while both of them significantly outperform the SMLD. By contrast, when the TZF/TRD-PSM systems are considered, the RTT-MLD is outperformed by the SMLD, when $M_d \geq 1$. This is because the TZF operation amplifies noise and makes the observations at different receive antennas become correlated. By contrast, when TMMSE is employed, the observations at different receive antennas are nearly uncorrelated and can be well approximated by the Gaussian distribution, which makes the RTT-MLD highly effective.

When comparing the results shown in Figs. 7 and 8, we explicitly witness the significant difference between the SMLD and the simplified SMLD, when $M_d \geq 1$. As shown in Fig. 7, for both the TZF/TRD-PSM and TMMSE/TRD-PSM systems, diversity gain can be achieved by increasing the number of diversity antennas. By contrast, when the simplified SMLD is employed, as shown in Fig. 8, the TMMSE/TRD-PSM system is capable of achieving some diversity gain in low SNR region,

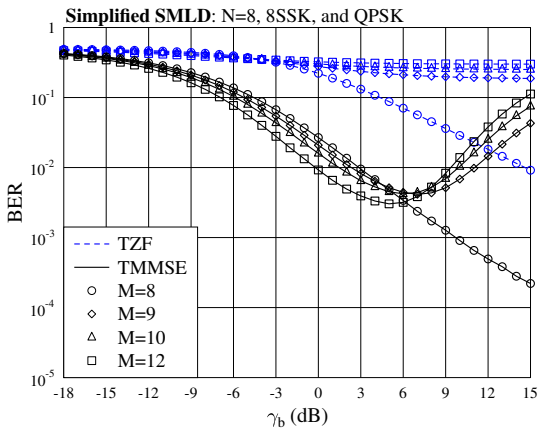

Fig. 8. BER versus average SNR per bit performance of the TRD-PSM systems with simplified SMLD of (23) and (26).

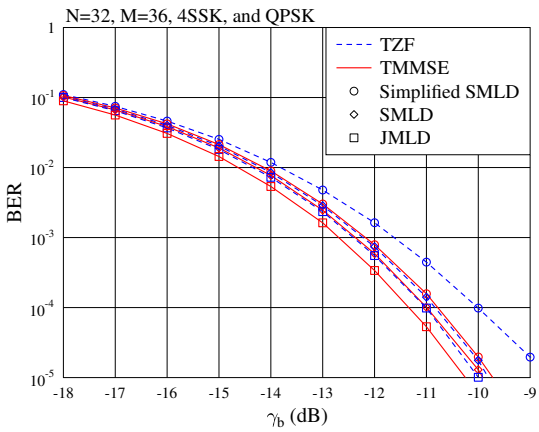

Fig. 9. Comparison of BER versus average SNR per bit performance of the SMLD, simplified SMLD and the JMLD.

but no diversity gain in high SNR region. For the TZF/TRD-PSM system, there is no diversity gain in the whole SNR region. The reason for the above observations is as follows. When comparing (21) and (23) in Section III-B, the simplified SMLD ignores the negative term of $-\|\boldsymbol{H}_d^T\boldsymbol{p}_{m_1'}\|^2/2$ used in the SMLD. This ignored term imposes interference on the M_d diversity antennas. When SNR is low, the BER performance is dominated by noise, making the TMMSE/TRD-PSM system achieve certain diversity gain. However, when SNR is high, the interference becomes overwhelming and, in this case, no diversity gain is available. From the above analysis we can know that the simplified SMLD, which has been widely employed in references [10, 11, 15, 16, 50, 51], is not suitable for the TRD-PSM systems.

In Fig. 8, $M_d = 0,\ 1,\ 2$ and 4 are considered, which are relatively small values. By contrast, Fig. 9 plots the BER performance of the TZF/TRD-PSM and TMMSE/TRD-PSM systems employing the SMLD, simplified SMLD as well as the benchmark JMLD, when M_d takes a relatively large value of $M_d = 36-4 = 32$. In this case, we can know from statistics theory that $\|\boldsymbol{H}_d^T\boldsymbol{p}_{m_1'}\|^2$ in (21) converges to a constant of $\mathbb{E}\left[\|\boldsymbol{H}_d^T\boldsymbol{p}_{m_1'}\|^2\right]$, which results in that the SMLD converges to the simplified SMLD expressed by (23). Consequently, as shown in Fig. 9, for either the TZF/TRD-PSM or the TMMSE/TRD-PSM, the BER performance achieved by the simplified SMLD becomes closer to that of the SMLD, when comparing to the results shown in Figs. 7 and 8. Furthermore, while the SMLD still outperforms the simplified SMLD, the BER performance attained by both of them is close to that achieved by the JMLD, especially when the TMMSE/TRD-PSM system is considered. Hence, for a TRD-PSM system employing a big number of diversity antennas, both the SMLD and the simplified SMLD are near optimum.

In Fig. 10, we demonstrate the approximate ABEP upper-bound of (42) derived in Section IV. In this example, both the pure PSM and the TRD-PSM systems are considered. We assume 4SSK and QPSK, and that the transmitter employs $N = 8$ antennas. Hence, for the pure PSM system, there are $M = 4$ receive antennas. By contrast, we assume that the TRD-PSM system is equipped with $M = 12$ receive antennas, corresponding to $M_d = 8$. As shown in Fig. 10, the BER as well as the upper-bound (UBound) results of both TZF/TRD-PSM and TMMSE/TRD-PSM systems are better than the corresponding BER and UBound results of the pure TZF-PSM (or TMMSE-PSM) systems. Straightforwardly, this is because the contribution made by the M_d extra receive antennas in the TRD-PSM systems. Note that, the performance advantage of the TRD-PSM systems over the pure PSM systems will also be witnessed in the forthcoming figures. As shown in Fig. 10, at a sufficiently high SNR, although the approximate ABEP upper-bound for the pure PSM is tighter than the corresponding ABEP upper-bound of the TRD-PSM, the upper-bounds for all the cases are in general tight. Hence, we can be convinced the effectiveness of both the Gamma-Ap and the approximation invoked for deriving the ABEP upper-bound of (42). Additionally, Fig. 10 shows that the ABEP upper-bound for the TMMSE/TRD-PSM is slightly tighter than that for the TZF/TRD-PSM. This is because the TMMSE results in more independent Gaussian-like observations than the TZF[4] [40].

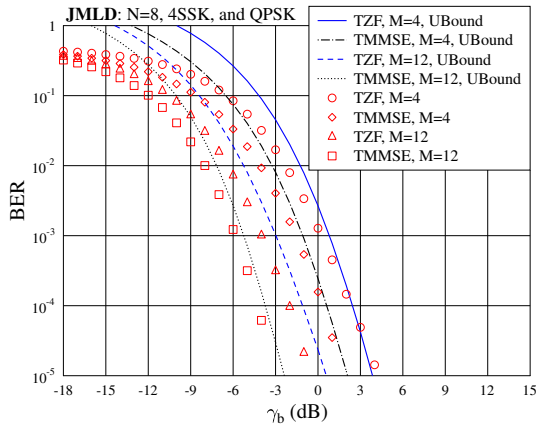

Fig. 10. Comparison between the simulated BER and the approximate ABEP upper-bounds of the TRD-PSM systems with JMLD.

In Fig. 11 and 12, we demonstrate the tightness of the asymptotic ABEP upper-bounds evaluated from (49), by comparing them with the simulated BER, when both the TZF/TRD-PSM and TMMSE/TRD-PSM systems with JMLD are considered. Specifically, Fig. 11(a) assumes $M = 4$ receive

[4]While ZF processing fully removes interference, it however makes noise samples become correlated.

antennas, meaning that there is no receive diversity, while Fig. 11(b) assumes $M = 36$, giving $M_d = 32$ and hence a high receive diversity order. The other parameters for both Fig. 11(a) and Fig. 11(b) are the same, as detailed in the figures. From Fig. 11 we observe that the upper-bounds are in general tight for all the cases considered in the high SNR region. By contrast, in the low SNR region, the ones in Fig. 11(b) are tighter than the corresponding ones in Fig. 11(a). Furthermore, we can see that using $M = 36$ instead of $M = 4$ receive antennas results in about 3 dB SNR gain at the BER of 10^{-5}. Note that, as there are $N = 32$ transmit antennas in the considered cases, which is significantly larger than $M = 4$ required for implementing the 4SSK, there is already a big diversity gain provided by the 28 extra transmit antennas. Due to this, the diversity gain provided by the $M_d = 32$ receive antennas is not remarkable. By contrast, in Fig. 12, we demonstrate the effect of the number of receive antennas on the tightness of the asymptotic ABEP upper-bound. Apparently, using $M_d = 64$ diversity antennas results in a tighter upper-bound than using no ($M_d = 0$) diversity antennas at receiver, especially, in the low SNR region.

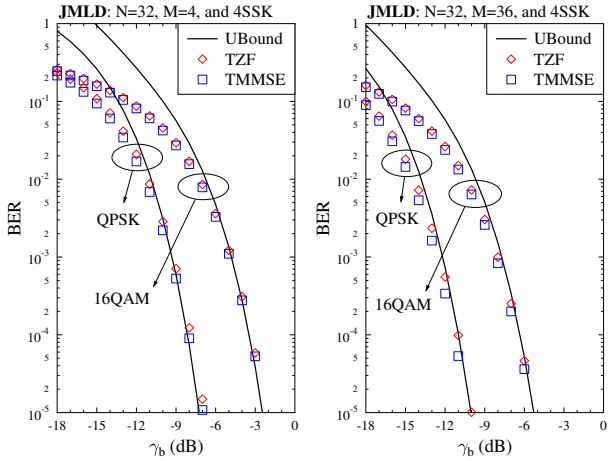

Fig. 11. Comparison between the simulated BER and the asymptotic ABEP upper-bounds for the TRD-PSM systems employing $N = 32$ transmit antennas and JMLD, when $M = 4$ (a) or $M = 36$ (b) receive antennas are employed.

From the results shown in Fig. 11 and 12, we are implied that the upper-bound of (49) derived in Section IV is valid, and can be used to estimate the BER performance of the PSM systems, provided that the SNR is sufficiently high, resulting in that the BER is about 10^{-3} or lower.

VI. Summary and Conclusions

We have proposed and studied a TRD-PSM MIMO transmission scheme, which is capable of achieving both transmit and receive diversity, and flexibly making use of CSIT. To implement PSM, two precoding schemes, namely TZF and TMMSE, have been studied, showing that they can reduce the transmitter's implementation complexity. In order to facilitate TRD-PSM to be implemented at different complexity, we have proposed and investigated a range of detectors, which include the JMLD, simplified JMLD, SMLD, simplified SMLD, and

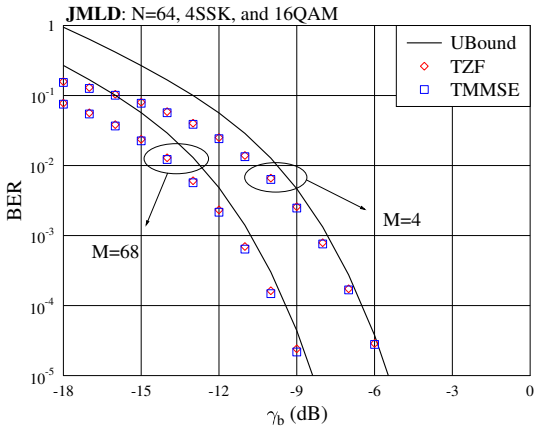

Fig. 12. Comparison between the simulated BER and the asymptotic ABEP upper-bounds for the TRD-PSM systems employing $N = 64$ transmit antennas and JMLD.

the RTT-MLD. Our studies demonstrate that, while the JMLD is capable of attaining the best error performance, it also has the highest complexity among the considered detectors. On the other hand, the simplified SMLD has the lowest implementation complexity but achieves the worst error performance among these detectors. The RTT-MLD can achieve a similar error performance as the simplified JMLD, which is close to that of the JMLD, while enjoying a significantly lower complexity than the simplified JMLD. We have demonstrated that the simplified SMLD, which has widely been studied in the references on SM, is inefficient for operation in PSM systems having extra receive antennas for diversity. Instead, the SMLD proposed in this paper is able to circumvent the problems of the simplified SMLD, and achieves desirable error performance.

We have also analyzed the ABEP of TRD-PSM systems employing respectively the JMLD and the simplified JMLD at both small- and large-scale. For the small-scale TRD-PSM systems, the approximate ABEP expressions have been derived via analyzing the union-bounds based on the Gamma-Ap. By contrast, for the large-scale TRD-PSM systems, the asymptotic ABEP formulas have been derived by invoking large-scale approximation. Our analytical results have been validated by simulations, and they demonstrate that the approximate and asymptotic ABEP expressions are general, and can be applied for evaluating the error performance of pure PSM systems.

Appendix

A. *Proof of Theorem 1*

As $\eta = v + w$ and v and w are uncorrelated, the mathematical expectation in (36) can be expressed as

$$\mathbb{E}_{\boldsymbol{H}}\left[g\left(v,w\right)\right] = \int_0^\infty g\left(\eta\right) f_\eta\left(\eta\right) d\eta \tag{54}$$

Substituting the PEP upper-bound of (35) and the PDF of (39) into the above equation, and making use of the formula

of (3.326,2) in [52], we obtain

$$\mathbb{E}_{\boldsymbol{H}}\left[g\left(v,w\right)\right] \approx \int_0^\infty \left(\frac{1}{6}e^{-\frac{\eta}{\sigma^2}}+\frac{1}{12}e^{-\frac{\eta}{2\sigma^2}}+\frac{1}{4}e^{-\frac{\eta}{4\sigma^2}}\right) \frac{1}{\Gamma\left(m_\eta\right)}\left(\Omega_\eta\right)^{-m_\eta}\eta^{m_\eta-1}e^{-\eta/\Omega_\eta}d\eta$$
$$= \frac{1}{6}\left[\frac{\sigma^2}{\Omega_\eta+\sigma^2}\right]^{m_\eta}+\frac{1}{12}\left[\frac{2\sigma^2}{\Omega_\eta+2\sigma^2}\right]^{m_\eta}+\frac{1}{4}\left[\frac{4\sigma^2}{\Omega_\eta+4\sigma^2}\right]^{m_\eta} \tag{55}$$

which can be expressed in the form of (41).

B. Proof of Theorem 2

When communicating over iid Rayleigh fading channels, using the fact that $\boldsymbol{H}_d$ is independent of $\boldsymbol{u}$ and the result in (63) of [46], we can deduce that

$$\mathbb{E}_{\boldsymbol{H}_d}\left[\exp\left(-\frac{\left\|\boldsymbol{H}_d^T\boldsymbol{u}\right\|^2}{\alpha_j}\right)\right]=\left(\frac{\alpha_j}{\left\|\boldsymbol{u}\right\|^2+\alpha_j}\right)^{M_d} \tag{56}$$

Substituting it into (47) yields

$$\begin{aligned}&\mathbb{E}_{\boldsymbol{H}}\left[g\left(v,w\right)\right]\\ &=\sum_{j=1}^{3}\tau_j\exp\left(-\frac{Nd_{mx}}{\alpha_j}\right)\mathbb{E}_{\boldsymbol{H}_1}\left[\left(\frac{\alpha_j}{\left\|\boldsymbol{u}\right\|^2+\alpha_j}\right)^{M_d}\right]\\ &\overset{(c)}{\approx}\sum_{j=1}^{3}\tau_j\exp\left(-\frac{Nd_{mx}}{\alpha_j}\right)\mathbb{E}_{\boldsymbol{H}_1}\left[\left(\frac{\alpha_j}{d_{mx}+\alpha_j}\right)^{M_d}\right]\end{aligned} \tag{57}$$

where the approximation at (c) holds due to the large-scale asymptotic result of $\boldsymbol{H}_1^T\boldsymbol{H}_1^*/N\approx\boldsymbol{I}_{M_1}$. Consequently, we have the closed-form formula of (48).

REFERENCES

[1] M. D. Renzo, H. Haas, and P. M. Grant, "Spatial modulation for multiple-antenna wireless systems: A survey," *IEEE Commun. Mag.*, vol. 49, no. 12, pp. 182–191, Dec. 2011.

[2] M. D. Renzo, H. Haas, and *et.al*, "Spatial modulation for generalized MIMO: Challenges, opportunities, and implementation," *Proc. IEEE*, vol. 102, no. 1, pp. 56–103, Jan. 2014.

[3] P. Yang, M. D. Renzo, and *et.al*, "Design guidelines for spatial modulation," *IEEE Commun. Sur. & Tutor.*, vol. 17, no. 1, pp. 6–26, Firstquarter 2015.

[4] P. Yang, Y. Xiao, and *et.al*, "Single-Carrier SM-MIMO: A promising design for broadband large-scale antenna systems," *IEEE Commun. Sur. & Tutor.*, vol. 18, no. 3, pp. 1687–1716, Thirdquarter 2016.

[5] Y. A. Chau and S. H. Yu, "Space modulation on wireless fading channels," in *Proc. of IEEE 54th VTC (Fall)*, Sep. 2001, pp. 1668–1671.

[6] R. Mesleh, H. Haas, and *et.al*, "Spatial modulation - a new low-complexity spectral efficiency enhancing technique," in *Proc. of Chinacom'2006*, Oct. 2006, pp. 1–5.

[7] S. Ganesan, R. Mesleh, and *et.al*, "On the performance of spatial modulation of OFDM," in *Proc. 40th Asilomar Conf. Signal, Syst. Comput.*, Oct. 29 - Nov. 1 2006, pp. 1825–1829.

[8] J. Jeganathan, A. Ghrayeb, and *et.al*, "Space shift keying modulation for MIMO channels," *IEEE Trans. Wireless Commun.*, vol. 8, no. 7, pp. 3692–3703, Jul. 2009.

[9] Y. Yang and B. Jiao, "Information-guided channel-hopping for high data rate wireless communication," *IEEE Commun. Lett.*, vol. 12, no. 4, pp. 225–227, Apr. 2008.

[10] R. Y. Mesleh, H. Haas, and *et.al*, "Spatial modulation," *IEEE Trans. Veh. Technol.*, vol. 57, no. 4, pp. 2228–2241, Jul. 2008.

[11] N. R. Naidoo, H. J. Xu, and T. A. M. Quazi, "Spatial modulation: Optimal detector asymptotic performance and multiple-stage detection," *IET Commun.*, vol. 5, no. 10, pp. 1368–1376, Jul. 2011.

[12] A. Garcia-Rodriguez and C. Masouros, "Low-complexity compressive sensing detection for spatial modulation in large-scale multiple access channels," *IEEE Transactions on Communications*, vol. 63, no. 7, pp. 2565–2579, July 2015.

[13] J. Wang, S. Jia, and J. Song, "Generalised spatial modulation system with multiple active transmit antennas and low complexity detection scheme," *IEEE Trans. Wireless Commun.*, vol. 11, no. 4, pp. 1605–1615, Apr. 2012.

[14] S. Sugiura, S. Chen, and L. Hanzo, "Coherent and differential space-time shift keying: A dispersion matrix approach," *IEEE Transactions on Communications*, vol. 58, no. 11, pp. 3219 – 3230, November 2010.

[15] A. Garcia-Rodriguez and C. Masouros, "Low-complexity compressive sensing detection for spatial modulation in large-scale multiple access channels," *IEEE Trans. Commun.*, vol. 63, no. 7, pp. 2565–2579, Jul. 2015.

[16] L.-L. Yang, "Signal detection in antenna-hopping space-division multiple-access systems with space-shift keying modulation," *IEEE Trans. Signal Process.*, vol. 60, no. 1, pp. 351–366, Jan. 2012.

[17] M. D. Renzo and H. Haas, "A general framework for performance analysis of space shift keying (SSK) modulation for MISO correlated Nakagami-m fading channels," *IEEE Trans. Commun.*, vol. 58, no. 9, pp. 2590–2603, Sep. 2010.

[18] ——, "Bit error probability of space modulation over Nakagami-m fading: Asymptotic analysis," *IEEE Commun. Lett.*, vol. 15, no. 10, pp. 1026–1028, Oct. 2011.

[19] ——, "Bit error probability of SM-MIMO over generalized fading channels," *IEEE Trans. Veh. Technol.*, vol. 61, no. 3, pp. 1124–1144, Mar. 2012.

[20] L.-L. Yang, "Transmitter preprocessing aided spatial modulation for multiple-input multiple-output systems," in *Proc. of IEEE 73th VTC (Spring)*, May 2011.

[21] A. Stavridis, M. D. Renzo, and H. Haas, "Performance analysis of multistream receive spatial modulation in the MIMO broadcast channel," *IEEE Trans. Wireless Commun.*, vol. 15, no. 3, pp. 1808–1820, Mar. 2016.

[22] A. Stavridis, M. D. Renzo, and *et.al*, "On the asymptotic performance of receive space modulation in the shadowing broadcast channel," *IEEE Commun. Lett.*, vol. 20, no. 10, pp. 2103–2106, Oct. 2016.

[23] A. Stavridis, M. D. Renzo, P. M. Grant, and H. Haas, "Performance analysis of receive space modulation in the shadowing MIMO broadcast channel," *IEEE Trans. Commun.*, vol. 65, no. 5, pp. 1972–1983, May 2017.

[24] C. Masouros and L. Hanzo, "Dual-Layered MIMO transmission for increased bandwidth efficiency," *IEEE Trans. Veh. Technol.*, vol. 65, no. 5, pp. 3139–3149, May 2016.

[25] A. Stavridis, D. Basnayaka, and *et.al*, "A virtual MIMO dual-hop architecture based on hybrid spatial modulation," *IEEE Trans. Wireless Commun.*, vol. 62, no. 9, pp. 3161–3179, Sep. 2014.

[26] R. Zhang, L.-L. Yang, and L. Hanzo, "Generalised pre-coding aided spatial modulation," *IEEE Trans. Wireless Commun.*, vol. 12, no. 11, pp. 5434–5443, Nov. 2013.

[27] ——, "Error probability and capacity analysis of generalised pre-coding aided spatial modulation," *IEEE Trans. Wireless Commun.*, vol. 14, no. 1, pp. 364–375, Jan. 2015.

[28] B. Gulbahar, "Network topology modulation for energy and data transmission in internet of magneto-inductive things," in *2016 IEEE Globecom Workshops*, Dec. 2016, pp. 1–6.

[29] J. Zheng, "Fast receive antenna subset selection for pre-coding aided spatial modulation," *IEEE Wireless Commun. Lett.*, vol. 4, no. 3, pp. 317–320, Jun. 2015.

[30] R. Zhang, L.-L. Yang, and L. Hanzo, "Performance analysis of non-linear generalized pre-coding aided spatial modulation," *IEEE Trans. Wireless Commun.*, vol. 15, no. 10, pp. 6731–6741, Oct. 2016.

[31] M. C. Lee, W. H. Chung, and T. S. Lee, "Generalized precoder design formulation and iterative algorithm for spatial modulation in MIMO systems with CSIT," *IEEE Trans. Commun.*, vol. 63, no. 4, pp. 1230–1244, Apr. 2015.

[32] P. Yang, Y. L. Guan, Y. Xiao, M. D. Renzo, S. Li, and L. Hanzo, "Transmit precoded spatial modulation: Maximizing the minimum euclidean distance versus minimizing the bit error ratio," *IEEE Trans. Wireless Commun.*, vol. 15, no. 3, pp. 2054–2068, Mar. 2016.

[33] C. Masouros and L. Hanzo, "Constellation randomization achieves transmit diversity for single-RF spatial modulation," *IEEE Trans. Veh. Technol.*, vol. 65, no. 10, pp. 8101–8111, Oct. 2016.

[34] M. C. Lee, W. H. Chung, and T. S. Lee, "Limited feedback precoder design for spatial modulation in MIMO systems," *IEEE Commun. Lett.*, vol. 19, no. 11, pp. 1909–1912, Nov. 2015.

[35] P. Yang, Y. Xiao, B. Zhang, S. Li, M. El-Hajjar, and L. Hanzo, "Power allocation-aided spatial modulation for limited-feedback MIMO systems," *IEEE Trans. Veh. Technol.*, vol. 64, no. 5, pp. 2198–2204, May 2015.

[36] A. J. Viterbi, "A robust ratio-threshold technique to mitigate tone and partial band jamming in coded MFSK systems," in *Proc. of IEEE Milit. Commun. Conf. Rec.*, Oct. 1982, pp. 22.4.1–22.4.5.

[37] L.-L. Yang and L. Hanzo, "Ratio statistic test assisted residue number system based parallel communication systems," in *Proc. of IEEE VTC'99*, Houston, USA, May 1999, pp. 894–898.

[38] ——, "Performance analysis of coded M-ary orthogonal signaling using errors-and-erasures decoding over frequency-selective fading channels," *IEEE J. Sel. Areas Commun.*, vol. 19, no. 2, Feb. 2001.

[39] ——, "Low complexity erasure insertion in RS-coded SFH spread-spectrum communications with partial-band interference and Nakagami-m fading," *IEEE Trans. Commun.*, vol. 50, no. 6, pp. 914–925, Jun. 2002.

[40] H. V. Poor and S. Verdu, "Probability of error in MMSE multiuser detection," *IEEE Trans. Inf. Theory*, vol. 43, no. 3, pp. 858–871, May 1997.

[41] M. D. Renzo and H. Haas, "Space shift keying (SSK) modulation with partial channel state information: Optimal detector and performance analysis over fading channels," *IEEE Trans. Commun.*, vol. 58, no. 11, pp. 3196–3210, Nov. 2010.

[42] H. L. V. Trees, *Optimum Array Processing*. Wiley Interscience, 2002.

[43] J. G. Proakis, *Digital Communications*, 5th ed. McGraw Hill, 2007.

[44] M. K. Simon and M.-S. Alouini, *Digital Communication over Fading Channels*, 2nd ed. New York: John Wiley & Sons, 2005.

[45] M. Chiani, D. Dardari, and M. K. Simon, "New exponential bounds and approximations for the computation of error probability in fading channels," *IEEE Trans. Wireless Commun.*, vol. 2, no. 4, pp. 840–845, Jul. 2003.

[46] W. Zeng, C. Xiao, and *et.al*, "Linear precoding for finite-alphabet inputs over MIMO fading channels with statistical CSI," *IEEE Trans. Signal Process.*, vol. 60, no. 6, pp. 3134–3148, Jun. 2012.

[47] A. Papoulis and S. U. Pillai, *Probability, Random Variables, and Stochastic Processes*, 4th ed. New York: McGraw-Hill, Inc, 2002.

[48] J. Shi, C. Dong, and L.-L. Yang, "Performance comparison of cooperative relay links with different relay processing strategies: Nakagami/gamma approximation approaches," *EURASIP J. Wireless Commun. Networ.*, vol. 2014, no. 1, pp. 1–17, 2014.

[49] L. Lu, G. Li, and *et.al*, "An overview of massive MIMO: Benefits and challenges," *IEEE J. Sel. Topics Signal Process.*, vol. 8, no. 5, pp. 742–758, Oct. 2014.

[50] S. Sugiura, C. Xu, and *et.al*, "Reduced-complexity coherent versus non-coherent QAM-aided space-time shift keying," *IEEE Trans. Commun.*, vol. 59, no. 11, pp. 3090–3101, Nov. 2011.

[51] P. Yang, Y. Xiao, and *et.al*, "An improved matched-filter based detection algorithm for space-time shift keying systems," *IEEE Signal Process. Lett.*, vol. 19, no. 5, pp. 271–274, May 2012.

[52] I. Gradshteyn and I. Ryzhik, *Table of Integrals, Series, and Products*, 7th ed. San Diego, C.A.: Academic Press, Inc, 2007.

Chaowen Liu received the B.S. degree in electrical engineering from Henan University of Science and Technology, Luoyang, China, in 2011. He is currently working towards the Ph.D. degree at the Institute of Information Engineering, Xi'an Jiaotong University, Xi'an, China. Since November 2015, he has been a Visiting Ph.D. Student with Prof. Lie-Liang Yang with the School of Electronics and Computer Science, University of Southampton, UK. His main research interests include spatial domain modulation techniques, physical layer security, full-duplex node aided wireless communications, index modulation for 5G wireless networks, and node-positioning in wireless sensor networks.

Lie-Liang Yang (M'98, SM'02, F'16) received his BEng degree in communications engineering from Shanghai TieDao University, Shanghai, China in 1988, and his MEng and PhD degrees in communications and electronics from Northern (Beijing) Jiaotong University, Beijing, China in 1991 and 1997, respectively. From June 1997 to December 1997 he was a visiting scientist of the Institute of Radio Engineering and Electronics, Academy of Sciences of the Czech Republic. Since December 1997, he has been with the University of Southampton, United Kingdom, where he is the professor of wireless communications in the School of Electronics and Computer Science. He has research interest in a wide range of topics in wireless communications, wireless networks and signal processing for wireless communications, as well as molecular communications. He has published over 330 research papers in journals and conference proceedings, authored/co-authored three books and also published several book chapters. The details about his publications can be found at http://www.mobile.ecs.soton.ac.uk/lly/. He is a fellow of both the IEEE and the IET, and a distinguished lecturer of the IEEE. He served as an associate editor to the IEEE Trans. on Vehicular Technology and Journal of Communications and Networks (JCN), and is currently an associate editor to the IEEE Access and the Security and Communication Networks (SCN) Journal.

Wenjie Wang (M'10) received the B.S., M.S., and Ph.D. degrees in information and communication engineering from Xi'an Jiaotong University, Xi'an, China, in 1993, 1998, and 2001, respectively. From 2009 to 2010, he was a visiting scholar at the Department of Electrical and Computer Engineering, University of Delaware, Newark, USA. Currently, he is a Professor at Xi'an Jiaotong University. His main research interests include information theory, broadband wireless communications, signal processing with application to communication systems, array signal processing and cooperative communications in distributed networks.